Seasonal persistence of circulation anomalies in the Southern Hemisphere stratosphere, and its implications for the troposphere

Article

Published Version

It is advisable to refer to the publisher's version if you intend to cite from the work. See Guidance on citing.

To link to this article DOI: http://dx.doi.org/10.1175/JCLI-D-17-0557.1

Publisher: American Meteorological Society

www.reading.ac.uk/centaur

CentAUR

Central Archive at the University of Reading

Reading's research outputs online

Seasonal Persistence of Circulation Anomalies in the Southern Hemisphere Stratosphere and Its Implications for the Troposphere

NICHOLAS J. BYRNE AND THEODORE G. SHEPHERD

Department of Meteorology, University of Reading, Reading, United Kingdom

ABSTRACT

Previous studies have highlighted an important organizing influence of the seasonal Southern Hemisphere stratospheric vortex breakdown on the large-scale stratospheric and tropospheric circulation. The present study extends this work by considering the statistical predictability of the stratospheric vortex breakdown event, using reanalysis data. Perturbations to the winter stratospheric vortex are shown to persist into austral spring and to lead to a shift in the statistics of the breakdown event during austral summer. This is interpreted as evidence for the potential for seasonal predictability of the vortex breakdown event in the stratosphere. Coupled variability between the stratosphere and troposphere is then considered. The semiannual oscillation of the tropospheric midlatitude jet is discussed, and evidence for a connection between this behavior and variations in the stratosphere is presented. Based on this connection, an argument is made for the concomitant potential for seasonal predictability in the troposphere, assuming knowledge of the stratospheric initial state. Combining these various results, a nonstationary, regime-based perspective of large-scale extratropical Southern Hemisphere circulation variability between late winter and summer is proposed. The implications of this perspective for some previous studies involving annular modes of the circulation are discussed. In particular, the long annular mode time scales during austral spring and summer should not be interpreted as an increased persistence of perturbations to some slowly varying seasonal cycle, but instead as a reflection of a phase shift of the seasonal cycle induced by stratospheric variability.

1. Introduction

Seasonal climate prediction is distinct from conventional weather forecasting in that it does not attempt to forecast the day-to-day evolution of weather. Instead it attempts to provide estimates of time-mean statistics, typically several months in advance (Palmer and Anderson 1994). The theoretical basis for such extended-range prediction is attributed to two fundamental constraints on the evolution of the atmosphere: the surface boundary conditions and the atmospheric initial conditions. Traditionally it has been the surface boundary conditions that have been the primary focus of attention. In particular, the phenomenon of El Niño–Southern Oscillation (ENSO) has formed the key paradigm for the design and implementation of many modern seasonal forecast systems (National Research Council 2010; Butler et al. 2016). More recently, evidence has been offered for the importance of the

atmospheric initial conditions (Stockdale et al. 2015), with the role of the stratospheric polar vortex receiving much attention. Much of this work has focused on the Northern Hemisphere (NH) and in particular on the influence of sudden stratospheric warmings (SSW) on the tropospheric circulation (Sigmond et al. 2013). However, there also exists a related body of work for the Southern Hemisphere (SH; Son et al. 2013; Seviour et al. 2014). SSW events are exceedingly rare in the SH (Roscoe et al. 2005), and so the source of this apparent skill requires a somewhat different explanation to that proposed for the NH.

The seasonal evolution of the SH stratospheric polar vortex (SSPV) exhibits several distinct features compared to its NH counterpart. In particular, the SSPV undergoes an annual downward shift in its location relative to its midwinter position (Hartmann et al. 1984). The shift-down behavior of the SSPV (Hio and Yoden 2005) typically proceeds from mid to late August and culminates in the vortex breakdown event sometime between mid-November and mid-January. The seasonal evolution of the SH tropospheric midlatitude

Corresponding author: Theodore G. Shepherd, theodore.shepherd@reading.ac.uk

jet/eddy-driven jet (EDJ) also exhibits several distinct features compared to its NH counterpart. In particular, the EDJ undergoes a semiannual oscillation (SAO) in latitude with the strongest winds closest to the pole in autumn and spring (van Loon 1967). The interannual variability of both of these components of the large-scale SH circulation was previously investigated by Kuroda and Kodera (1998), who documented an apparently coupled relationship between the SSPV and EDJ from midwinter until the vortex breakdown event in summer. These authors noted that during this period the variability of the coupled system appeared to be an "interannual phenomenon with a well-defined intraseasonal structure." This work was further extended by Hio and Yoden (2005), who noted two distinct configurations for the late winter SSPV and who referred to a "seasonal march" of the coupled variability. These authors conditioned their analysis on the late winter configuration of the SSPV and presented evidence that between August and December, the time-mean statistics of the large-scale extratropical tropospheric and stratospheric circulations were a function of this late winter configuration. A potential link between the stratospheric quasi-biennial oscillation (QBO) and the configuration of the winter SSPV was also investigated by both Kuroda and Kodera (1998) and Hio and Yoden (2005).

More recently, evidence has been presented of an equatorward transition of the EDJ in association with the stratospheric vortex breakdown event (Byrne et al. 2017), with the timing of this transition representing a leading-order influence on large-scale tropospheric circulation variability during this time of year. Figure 1 illustrates the extent of this influence: 500-hPa geopotential height anomalies averaged over the summer months are correlated against the date of the stratospheric vortex breakdown for each year during the satellite era. The significant correlation values at high latitudes are indicative of the impact of year-to-year variability in the timing of the vortex breakdown event in the stratosphere on tropospheric circulation anomalies [see Tripathi et al. (2015) for a review of some of the potential dynamical mechanisms involved in this coupling]. A natural question that emerges from this work is to ask how predictable (in a seasonal forecasting sense) the timing of this event might be, and how it relates to the earlier work of Kuroda and Kodera (1998) and Hio and Yoden (2005). It is also of interest to try to understand how these results might relate to the annular modes of the circulation, which in recent years have become the de facto choice for diagnosing stratosphere–troposphere coupling and the associated prospects for seasonal forecasting (e.g., Kidston et al.

2015, and references therein). The annular modes represent the dominant patterns of extratropical circulation variability in both hemispheres and correspond to a latitudinal shift of the EDJ in the troposphere and to a change in strength of the stratospheric polar vortex in the stratosphere (Thompson and Wallace 2000).

The present paper is an attempt at investigating these questions, using reanalysis data. It begins by exploring the extent to which the date of the stratospheric vortex breakdown is statistically predictable. This is done by relating interannual variations in the timing of the breakdown event to persistent variations of the SSPV in the preceding winter and spring. Coupled variability between the stratosphere and troposphere is then considered, and an argument is made for the concomitant potential for skillful seasonal forecasting in the troposphere. Based on these results a nonstationary, regime-based perspective of large-scale extratropical SH circulation variability between late winter and summer is proposed. The paper concludes with a summary of results and a discussion of possible future work.

2. Data and methods

The basic data input for our study is four-times-daily zonal wind and geopotential data from the ERA-Interim dataset for the period 1 March 1979 to 28 February 2017 (Dee et al. 2011). This period encompasses 38 years in the SH in total. Data were available on an N128 Gaussian grid and on 37 pressure levels (1000–1 hPa). Before analyzing the data, we first processed them by forming a daily and zonal average of the data. This processed data formed the input for all of our subsequent analysis. We define a climatology of our data as the long-term daily average that is subsequently smoothed by retaining the first six Fourier harmonics (Black and McDaniel 2007). We define a daily jet latitude index by vertically averaging zonal-mean daily mean zonal wind data between 1000 and 250 hPa, and subsequently computing the latitude of the maximum value of this average between 0° and 90°S (Byrne et al. 2017). We identify the date of the stratospheric vortex breakdown as the final time that the zonal-mean daily mean zonal wind at 60°S drops below $10\,\mathrm{m\,s^{-1}}$; we apply this criterion to running 5-day averages at 50 hPa (Black and McDaniel 2007). We use 60°S as the boundary for our polar-cap average. We define the phase of the QBO using the sign of July monthly mean zonal-mean zonal wind at 20 hPa averaged between 5°N and 5°S (Anstey and Shepherd 2014). We define our SAO index as the difference between monthly
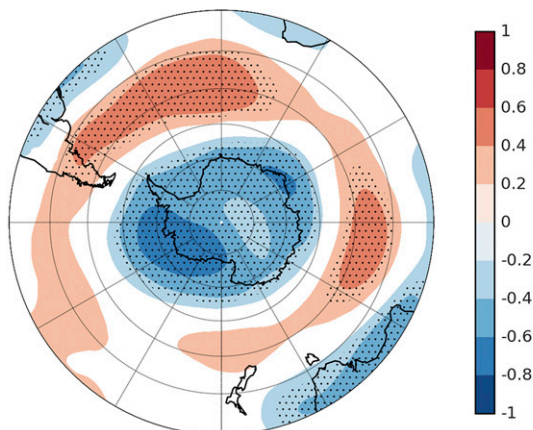
500hPa Geopotential Height (DJF 1979 - 2016)

FIG. 1. Correlation values between DJF 500-hPa geopotential height anomalies and the date of the stratospheric vortex breakdown during the satellite era. All data have been linearly detrended prior to calculation of correlation values. Stippled regions represent correlation values that are statistically significant at the 5% level, based on a two-sided Student's t test. Correlation values between -0.2 and 0.2 are colored white for presentation purposes.

mean zonally averaged sea level pressure at 50° and 65°S (Bracegirdle 2011). We define our annular mode index for each pressure level of our data in a similar manner to Baldwin and Thompson (2009). First, we compute daily anomaly data of zonal-mean daily mean geopotential height by removing a daily climatology. Next, we perform an empirical orthogonal function (EOF) analysis between 20° and 90°S and at each individual level; we weight our data to account for the decrease in area toward the pole (North et al. 1982). Finally we define our annular mode index as the normalized principal component time series that results from our EOF analysis. For our annular mode composite analysis we consider years with the 13 largest positive and 13 largest negative values in our annular mode index at 30 hPa. These represent approximately the upper and lower terciles of our data. We composite about an onset date that is defined as the day when anomalies in the annular mode index at 30 hPa cross the two-standard-deviation threshold for the final time prior to the peak of the event (Thompson et al. 2005).

3. Stratospheric circulation variability

a. Climatology and interannual variability

The shift-down of the SSPV typically proceeds from mid to late August (Hartmann et al. 1984). Long-term monthly average plots of zonal-mean zonal wind [u] are plotted from August in Fig. 2. Clear evidence of the downward progression and a general weakening of the

winds can be seen in this figure.[1] There is also a suggestion of something of a merger with the tropospheric EDJ and a tilting of the SSPV from late September onward. The downward progression of the SSPV continues until the final vortex breakdown event, which occurs every year sometime between mid-November and mid-January. The year of 2002 is a notable exception to this description as it was associated with the only documented SSW in the SH during the observational record; in 2002 the downward progression of the SSPV was substantially accelerated relative to its usual behavior (e.g., Hio and Yoden 2005). Interannual variations in the SSPV life cycle, such as those seen in 2002, were previously investigated by Kuroda and Kodera (1998) and Hio and Yoden (2005) by means of a multiple EOF analysis on zonal-mean zonal wind. We employ a similar method using polar-cap-averaged geopotential height at 30 hPa. The use of polar-cap-averaged geopotential height allows us to relate our results more directly to the annular mode indices that are considered later in the paper.

Figure 3a shows the seasonal evolution of polar-cap-averaged geopotential height at 30 hPa. It is plotted from March through February as the vortex occasionally persists into January in the lower regions of the stratosphere. Interannual variability is seen to be largest from August until January. The exceptional year of 2002 is also plotted for comparison. To perform a multiple EOF analysis on our 38-yr dataset we proceed by combining 12 months of data (starting from March) in a vector $\mathbf{x}^i$ as follows:

$$\mathbf{x}^i = [Z^i(1), \ldots, Z^i(12)]^T , \qquad (1)$$

where $Z^i(m)$ is the anomalous monthly averaged polar-cap-averaged geopotential height at 30 hPa for the mth month of the ith year. The leading modes of variability are then extracted as the eigenvectors of the covariance matrix calculated from $\mathbf{x}^i$. The leading mode (EOF1) is shown in Fig. 3b. This leading mode explains over 73% of the total variance and is clearly separated from the second EOF (North et al. 1982). Its monopolar structure suggests that for a year where a strong or weak SSPV develops in winter (negative or positive polar-cap-average geopotential height anomalies, respectively), it will tend to

---

[1] Inspection of individual years reveals that the downward progression occurs concurrently with transient vacillations in the magnitude of [u], which are associated with the development of eastward-traveling anticyclones about the polar vortex (e.g., Hio and Yoden 2004, and references therein). As the present paper is exclusively concerned with an analysis of the zonal-mean circulation, we do not document this three-dimensional behavior further.
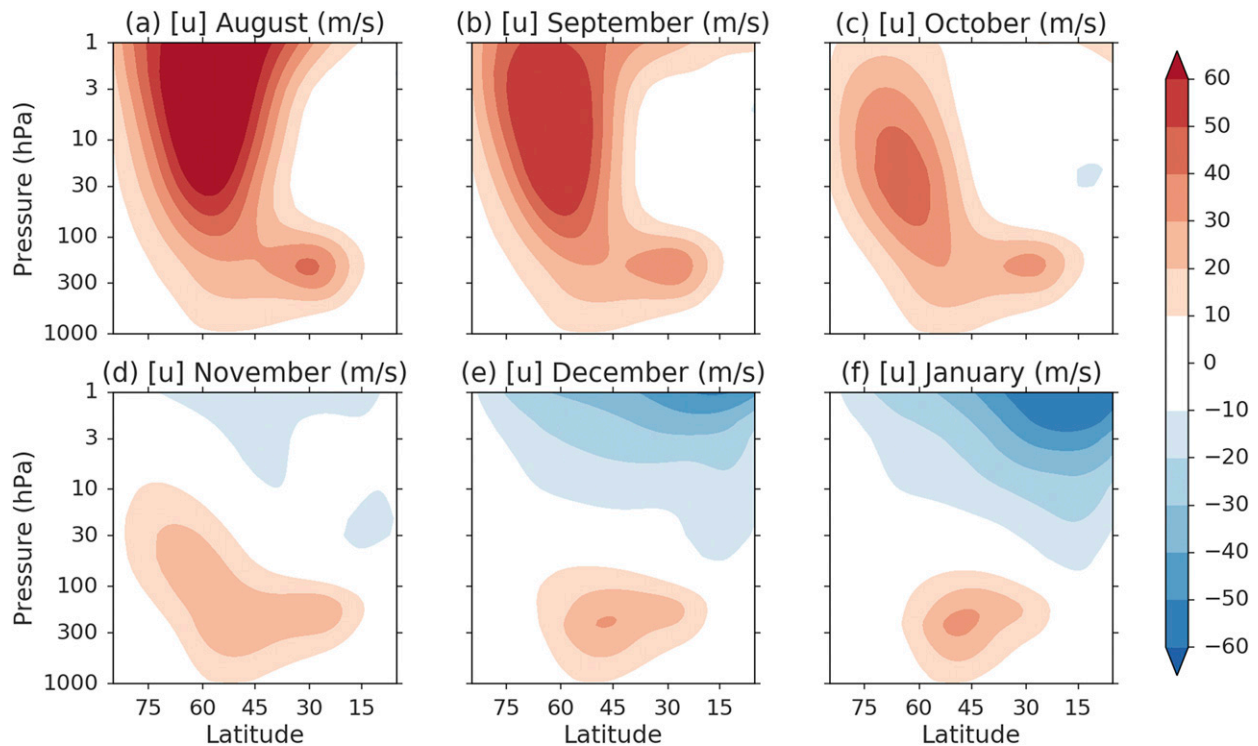
FIG. 2. Monthly mean climatologies of [u].

persist for the remainder of the SSPV life cycle until the vortex breakdown event in summer (see also Gerber et al. 2010). The principal component (PC1) time series of EOF1 is shown in Fig. 4. Weak (W) SSPV years are associated with a positive PC1 value and strong (S) SSPV years are associated with a negative value. Inspection of this plot reveals that the extreme values of PC1 (defined as the upper and lower quartiles of the data) are distributed in a somewhat specific manner. In particular, the extreme values are clustered in the
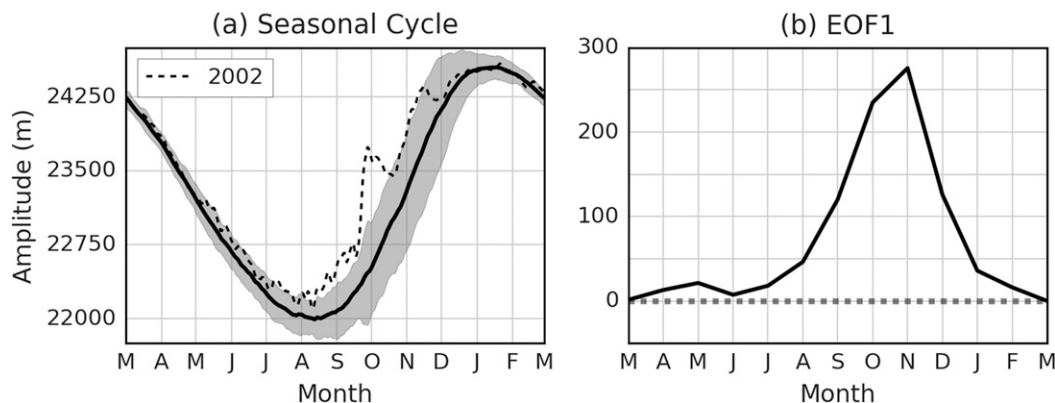

FIG. 3. (a) Seasonal cycle of polar-cap-averaged geopotential height at 30 hPa (thick black line). Shading represents a ±2-standard-deviations interval for each day of the year. Dashed line represents daily values during the year 2002. (b) EOF1 (m) from multiple EOF analysis on polar-cap-averaged geopotential height at 30 hPa (see text). The EOF represents the anomaly associated with one standard deviation of the principal component time series.
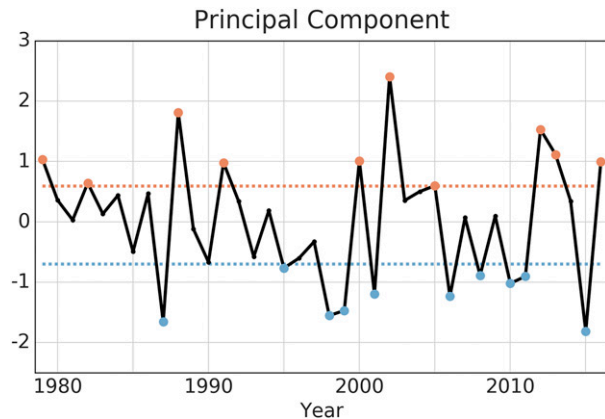
FIG. 4. Principal component time series of EOF1. The 10 largest positive (orange dots) and negative (blue dots) years are also plotted, along with the threshold values for these extreme years (dashed lines).

second half of the dataset, and there is a tendency for extreme positive years to directly follow extreme negative years. We have made an attempt at quantifying the significance of these features in the appendix ($p \sim 0.02$ and $p \sim 0.06$, respectively); we discuss potential explanations in section 5.

To explore how the EOF picture of interannual variability relates to the long-term-average behavior described earlier, we follow Hio and Yoden (2005) and perform a composite analysis on zonal-mean zonal wind using the W and S years of our PC1 index. We do this by forming monthly averages of [u] for W and S years separately and then calculating the difference between them. The results are presented in Fig. 5. The principal difference between the composites is that the entire downward progression of the SSPV is delayed in S years compared to W years. This delay results in a later average stratospheric vortex breakdown date (BD) in S years (16 December vs 30 November). It has been suggested that the dynamics of late breakdown events differ from those of early breakdown events (e.g., Sun et al. 2014; Byrne et al. 2017), and this may explain the differences in January. A more modest difference between the composites is that the SSPV appears stronger in S years (as measured by inspection of the meridional gradients of [u] on the equatorward flank of the SSPV). This difference in strength is beyond that which can be accounted for by a simple translation in time between the composites. The most noticeable impact of this difference in strength is on the tilting of the SSPV during
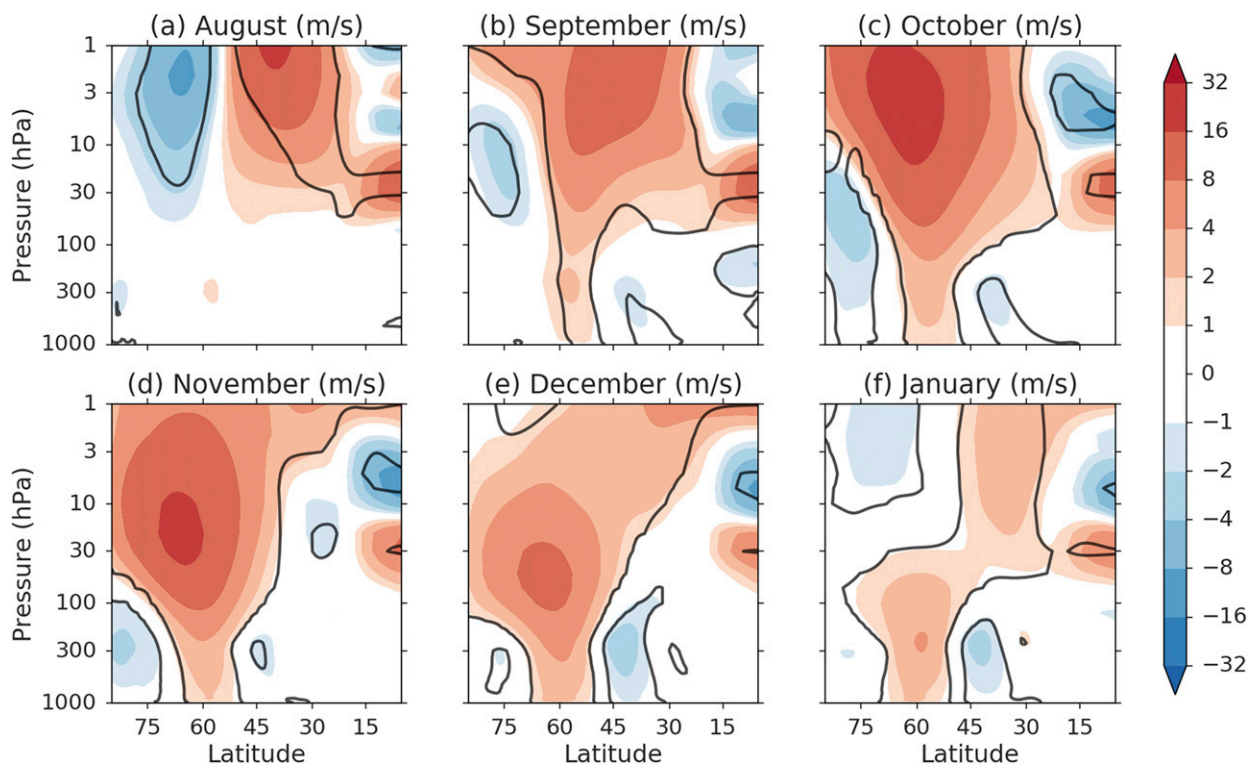

FIG. 5. Monthly mean differences in [u] between S and W years (color shading). Black contours represent regions where differences are statistically significant at the 5% level, based on a one-sided two-sample Student's t test. Note the nonlinear color scale that is required for including tropospheric and stratospheric differences in the same figure.
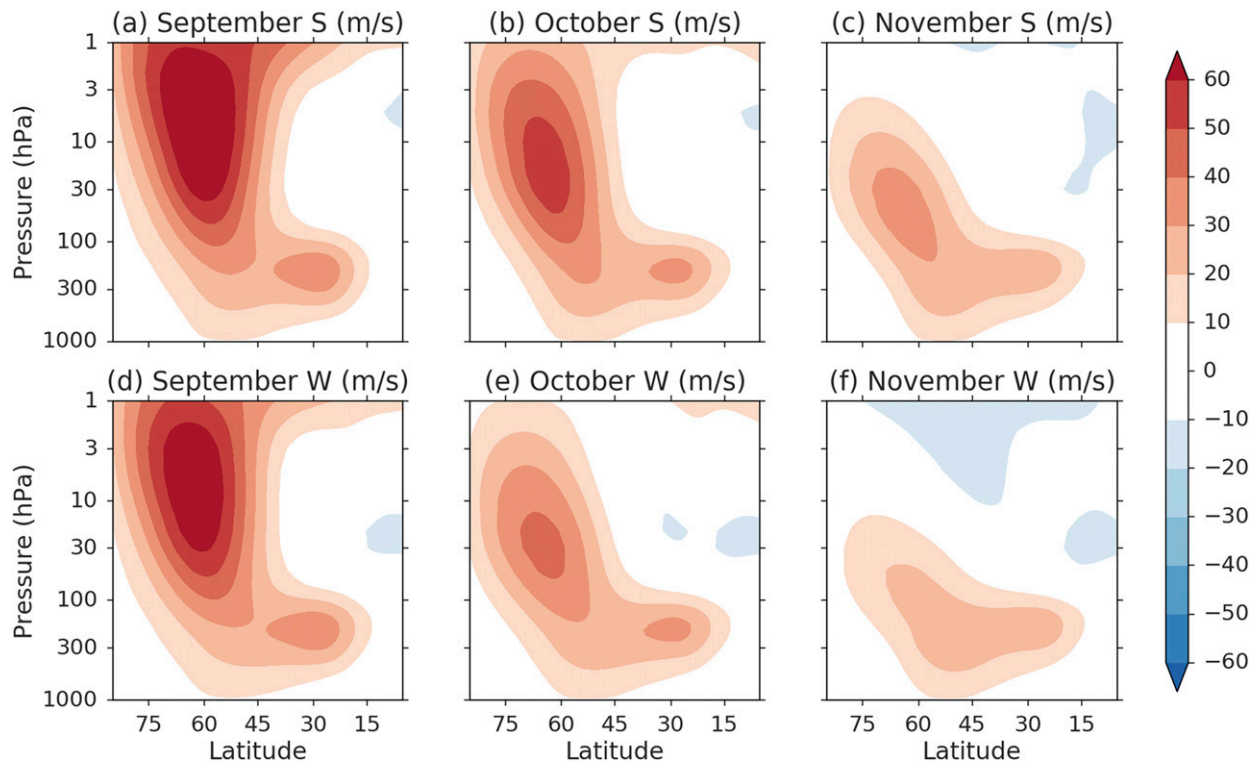
FIG. 6. (left to right) September through November mean [*u*] for (top) S and (bottom) W years.

October. This can be seen more clearly in Fig. 6, where monthly average plots for W and S years are shown separately. During October, the SSPV undergoes a relatively rapid weakening and tilting of the winds in W years, whereas it is more resilient to this weakening and tilting in S years. The S years are also associated with an extension of the strongest winds of the SSPV into the upper troposphere. This extension into the upper troposphere gives the appearance of something of a merger between the SSPV and the tropospheric EDJ; we return to the tropospheric impacts in more detail in section 4. Overall, it would appear that interannual variations between August and February can be largely described as a phase delay of the SSPV life cycle in S years, with changes to the amplitude of the life cycle (SSPV strength) a nonnegligible secondary effect.

b. Seasonal persistence of SSPV anomalies

The results of the previous section suggest that perturbations to the SSPV during winter can persist until the vortex breakdown event in summer. To investigate this potential predictive capability of the SSPV we employ a procedure suggested by Fioletov and Shepherd (2003) for total column ozone and compute correlation coefficients between a measure of the SSPV at a given month of the year and at subsequent months

(see Fig. 7). We use polar-cap-averaged geopotential height at 30 hPa as our SSPV measure, and we remove the year of 2002 from this correlation analysis owing to its outlier nature. Furthermore, we also linearly detrend all our data prior to analysis as the Southern Hemisphere stratosphere has been influenced by a well-documented trend in ozone [see Thompson et al. (2011) and references therein]. This influence is most clearly visible in a long-term trend for the breakdown date of the SSPV [see Byrne et al. (2017) and references therein].

Inspection of Fig. 7 suggests that SSPV predictability is considerable, particularly between the months of September and January. Predictability is seen to develop from August, with the longest period of predictability emerging around October, consistent with the peak of EOF1 in Fig. 3b. Correlation values above 0.6 are found for November, December, and January based on knowledge of the state of the SSPV in October. Predictability then decays following this October peak. These results are consistent with a hypothesis that perturbations to the SSPV in winter can lead to a shift in the statistics of the vortex breakdown event in the following summer. We have also made a separate attempt at quantifying this statement by constructing a linear predictor model for the SSPV breakdown date for each year
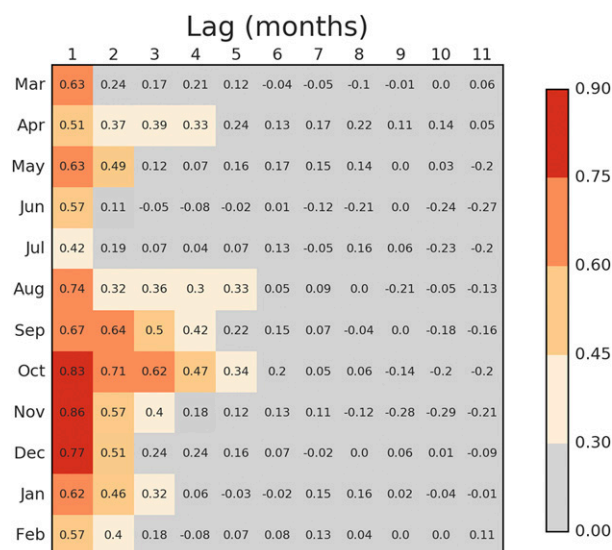
FIG. 7. Correlation coefficients between polar-cap-averaged 30-hPa geopotential height at a given month of the year with values in the subsequent months. For example, the correlation coefficient between polar-cap-averaged geopotential height in March and in the subsequent April is shown in the first column for March. Data have been linearly detrended for each month prior to calculation. Cells that are not shaded gray represent values that are statistically significant at the approximate 5% level based on a one-sided Student's t test. The year 2002 is not included in the correlation analysis (see text).

based on monthly mean polar-cap-averaged geopotential height at 30 hPa (Fig. 8). A statistically significant relationship is seen to exist between these two quantities from August, providing further evidence that perturbations to the SSPV in winter can lead to a shift in the statistics of the vortex breakdown event in the following summer.

Another means of exploring the association between perturbations to the SSPV life cycle and the vortex breakdown date involves the use of a graphical method previously suggested by Hirano et al. (2016), building on the "abacus plots" of Hitchcock et al. (2013). Polar-cap-averaged geopotential height anomalies at 30 hPa are computed for each day between 1 September and 1 February and are used to construct yearly time series. The yearly time series are then arranged chronologically by breakdown date. The result is plotted in Fig. 9. To a first approximation the figure is seen to be in reasonable agreement with the previous analysis: the latest breakdown dates are associated with a strong SSPV in the preceding months, while the opposite is found for the earliest breakdown dates. Closer inspection suggests two further features of interest. First, evidence of a strong SSPV is often seen to emerge at 30 hPa by 1 September, and this behavior would appear

to largely persist until the vortex breakdown event in summer; in contrast, evidence of a weakened SSPV is occasionally not seen to emerge until late September. It may be the case that some weak SSPV years are more clearly understood in terms of a single dynamical event (e.g., 1982; see Newman 1986). This may be suggestive of a fundamental asymmetry between weak and strong vortex years, perhaps related to the inherently dynamical nature of weak vortex years, with subsequent implications for the predictability time scale of the vortex breakdown event in weak SSPV years. However, confirmation of this statement is likely to be outside the scope of what is possible based on reanalyses.

The second feature that emerges from inspection of Fig. 9 is that occasionally years with a weak SSPV are associated with a somewhat delayed vortex breakdown date, with opposite behavior for years with a strong SSPV. From inspection of the particular examples for weak SSPV events, it appears that years with a large vortex weakening can occasionally be associated with a brief recovery of the vortex in late spring. The years of 2007 and 2014 are the outstanding examples of this behavior. From inspection of the particular examples for strong SSPV events, it appears that as the SSPV nears the end of its life cycle it can occasionally break down rather dramatically. The years of 1980 and 1997 are the outstanding examples of this behavior. While these exceptional years are not sufficient to affect the qualitative conclusions of our analysis, they may be of interest for seasonal forecasting applications, where a quantitative assessment is more important. Figure 9 suggests that forecasts which have been initialized sometime in early November may be able to capture the breakdown behavior in these years. It should be noted that the potential benefits of forecasts initialized in November need not be restricted to the short to medium range, as the timing of the breakdown event represents a leading-order influence on large-scale circulation variability during November, December, and even January (Sun et al. 2014; Byrne et al. 2017; see Fig. 1).

Before concluding this section, we also consider the role of the QBO, as previous research has suggested a potential for the QBO to perturb the SSPV life cycle during winter (e.g., Baldwin and Dunkerton 1998; Anstey and Shepherd 2014). We proceed by repeating our composite analysis from the previous section using July monthly mean winds at 20 hPa to define the phase of the QBO (Anstey and Shepherd 2014; see Table 1); we again remove the year 2002 from our analysis due to its outlier nature. The results of our analysis are shown in Fig. 10. Based on inspection of the individual months
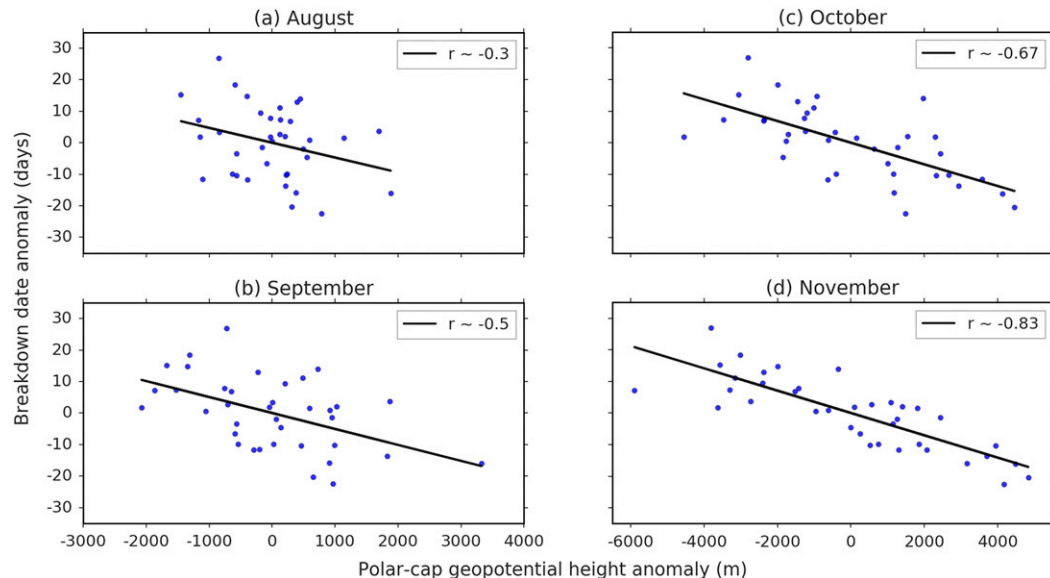
FIG. 8. Variations in the date of the stratospheric vortex breakdown regressed against monthly mean polar-cap-averaged geopotential height at 30 hPa for (a) August, (b) September, (c) October, and (d) November. All data have been linearly detrended prior to calculation. Correlation values for each month are located in the top right-hand corner of each plot. All correlation values are statistically significant at the 5% level, based on the one-sided Student's t test. The year 2002 is not included in the correlation analysis (see text).

of this figure it would appear that there is indeed an association between perturbations to the SSPV life cycle and the phase of the QBO, with weak SSPV years associated with an easterly winter QBO and strong SSPV years associated with a westerly winter QBO. As an alternative measure of this association we also test whether there is evidence of a statistical relationship between our PC1 index from section 3 and the phase of

the QBO (see the appendix). The results are suggestive of an association ($p \sim 0.06$), although our sample size again limits the statistical power of our analysis. Thus, it would appear likely that there is an association between the phase of the QBO and perturbations to the SSPV life cycle, although the strength of this association is not so large that it can be clearly detected in small sample sizes.
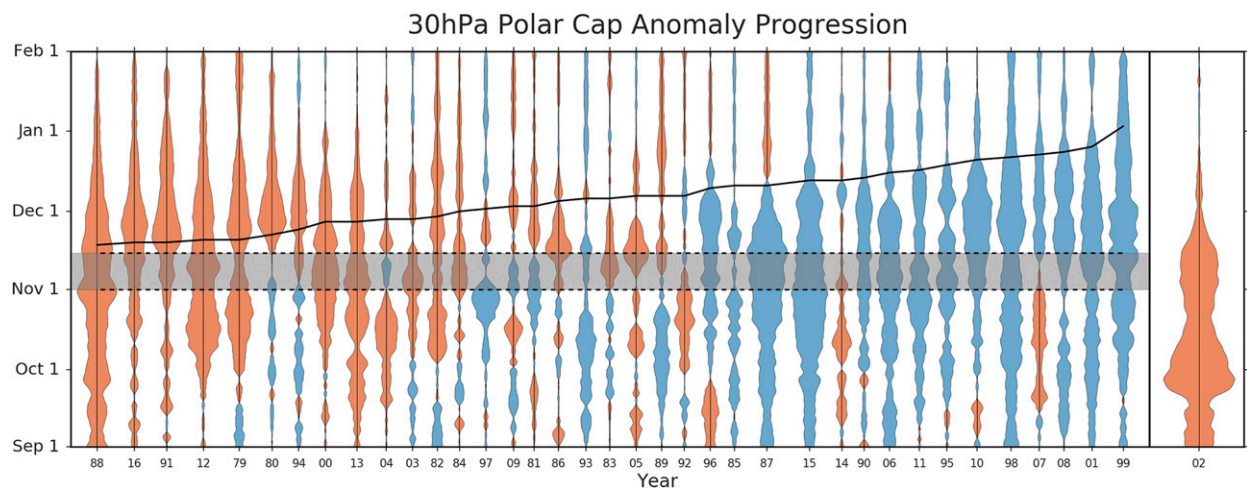

FIG. 9. Yearly time series of polar-cap-averaged geopotential height anomalies (m) at 30 hPa. Positive anomalies are orange and negative anomalies are blue. For reference, the anomaly on 1 Nov 1988 is approximately +700 m. The shaded regions indicate the suggested period for reinitialization of a forecast model (see text). The black line indicates the stratospheric vortex breakdown date for each year. The year 2002 is plotted separately on the right (see text).

TABLE 1. Classification of 38 yr based on PC1 (Fig. 4) along with classifications for the QBO and the breakdown date of the SSPV. For PC1, W is a weak SSPV year and S is a strong SSPV year. For the QBO, E represents easterly monthly mean zonal wind values for July at 20 hPa and W represents westerly values. The values in parentheses denote actual monthly mean values according to the ERA-Interim product. For the SSPV BD (Byrne et al. 2017), E represents extreme early years, L represents extreme late years, e represents extreme years before the median breakdown date, and l represents years after the median breakdown date. Breakdown dates for each year are shown in parentheses.

Year	1979	1980	1981	1982	1983	1984	1985	1986	1987	1988	1989	1990	1991
PC1	W	W	W	W	W	W	S	W	S	W	S	S	W
QBO (20 hPa)	E (−33)	W (16)	E (−28)	W (6)	E (−26)	E (−29)	W (12)	E (−30)	W (6)	E (−28)	E (−36)	W (17)	E (−27)
BD	E (20 Nov)	E (22 Nov)	e (3 Dec)	e (29 Nov)	e (6 Dec)	e (1 Dec)	l (11 Dec)	e (5 Dec)	l (11 Dec)	E (18 Nov)	l (7 Dec)	L (14 Dec)	E (19 Nov)

Year	1992	1993	1994	1995	1996	1997	1998	1999	2000	2001	2002	2003	2004
PC1	W	S	W	W	S	S	S	S	W	S	W	W	W
QBO (20 hPa)	W (8)	E (−23)	E (−26)	W (11)	E (−35)	W (14)	E (−29)	W (8)	E (−37)	E (−11)	E (−6)	E (−29)	W (8)
BD	1 (7 Dec)	l (6 Dec)	E (24 Nov)	L (19 Dec)	l (10 Dec)	e (2 Dec)	L (22 Dec)	L (3 Jan)	E (27 Nov)	L (26 Dec)	e (3 Dec)	e (28 Nov)	E (28 Nov)

Year	2005	2006	2007	2008	2009	2010	2011	2012	2013	2014	2015	2016
PC1	W	S	W	S	W	S	S	W	W	W	S	W
QBO (20 hPa)	E (−34)	W (13)	E (−33)	W (11)	E (−33)	W (8)	E (−26)	E (−20)	W (16)	E (−29)	W (15)	W (9)
BD	1 (7 Dec)	L (16 Dec)	L (23 Dec)	L (24 Dec)	e (3 Dec)	L (21 Dec)	L (17 Dec)	E (20 Nov)	E (27 Nov)	1 (13 Dec)	1 (13 Dec)	E (19 Nov)

4. Stratosphere–troposphere coupling

a. Interannual variations

The results of the previous section suggest that there is the potential for skillful seasonal forecasting in the SH stratosphere between August and February at least. As was highlighted in the references in the introduction, stratosphere–troposphere coupling in the SH has been regularly documented for this time of year. Thus we now consider whether there is also evidence for the potential for skillful seasonal forecasting in the troposphere, based on knowledge of the initial stratospheric state. We begin by describing the long-term behavior of the tropospheric EDJ using two separate measures. For our first measure we use vertically averaged zonal-mean zonal wind between 1000 and 250 hPa, denoted $\langle[u]\rangle$ (Byrne et al. 2017). For our second measure we use the difference in zonal-mean sea level pressure between 50° and 65°S (ZI) (Bracegirdle 2011); this difference in sea level pressure can be viewed as the SH equivalent to the NH zonal index (Kidson 1988). Long-term averages for both of these measures are shown in Fig. 11 and Fig. 12a. Inspection of these figures reveals a clear semiannual oscillation in the location of the EDJ, with the strongest winds closest to the pole in late March and October. As the present paper is concerned primarily with coupled stratosphere–troposphere behavior from late winter, we now restrict our attention to describing EDJ behavior between August and February.

From August until late September the long-term-average location of the EDJ undergoes little change. Starting from about late September, the EDJ transitions poleward until early November. This poleward transition of the EDJ is also associated with an intensification of the winds. Inspection of individual years suggests that this picture of a more poleward and intense EDJ in October is a reasonable description, although the intensification of the winds is more pronounced in some years than in others. The years of 1988 and 2002 are two clear exceptions to this description (not shown), both having very clearly defined equatorward jets. These years are also notable as having the two largest values in our PC1 index of stratospheric variability (Fig. 4). Large stratospheric variations during these years were associated with a vigorous minor warming (Hirota et al. 1990) and an SSW event, respectively. From about mid-November onward the EDJ undergoes an equatorward transition. This equatorward transition has been the focus of a previous study (Byrne et al. 2017), and we refer the reader to that paper for more details.
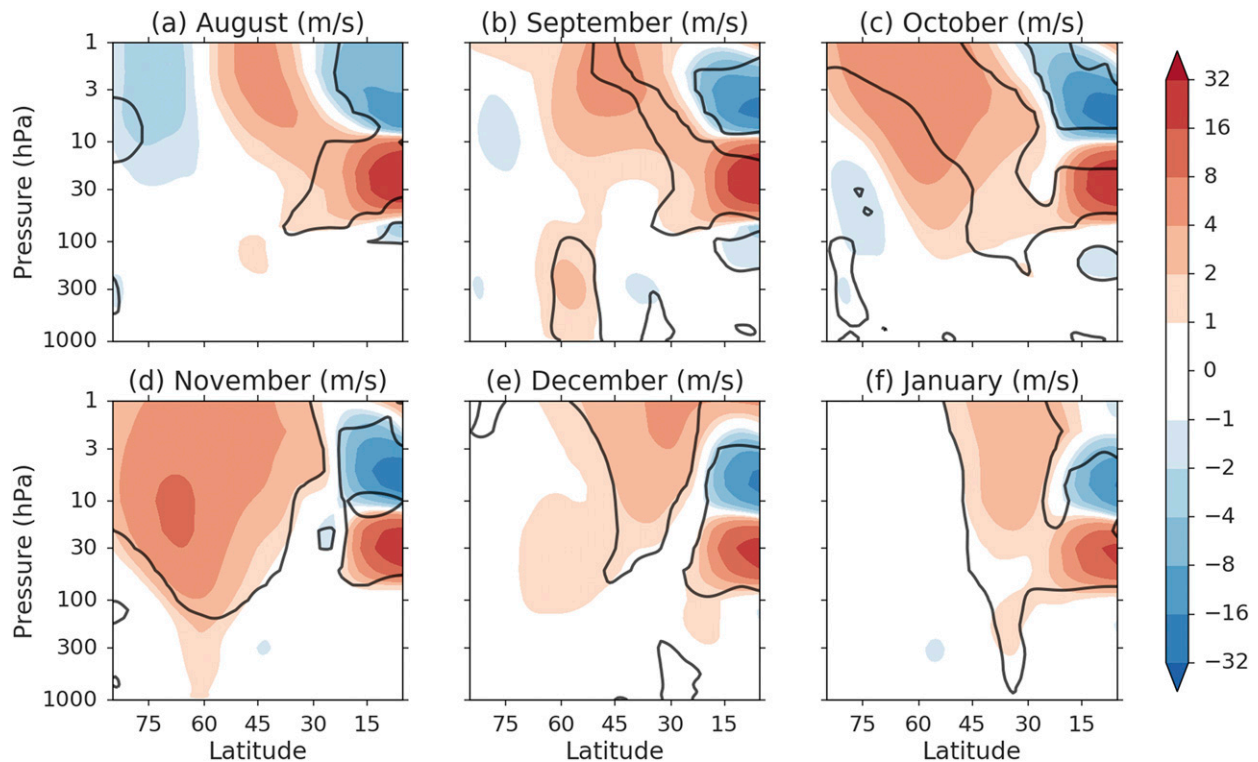
FIG. 10. (a)–(f) August through January mean differences in [*u*] between westerly and easterly QBO phase (color shading). The year 2002 is not included in the analysis (see text). Black contours represent regions where differences are statistically significant at the 5% level, based on a one-sided two-sample Student's *t* test. Note the nonlinear color scale required for including tropospheric and stratospheric differences in the same figure.

Broadly speaking, it reflects a shift in latitude of the EDJ in association with the vortex breakdown in the stratosphere.

To investigate the potential for interannual variations in the stratosphere to impact the troposphere, we begin by revisiting Fig. 5. In the troposphere, statistically significant differences between W and S years are present from September through January, consistent with the earlier results of Hio and Yoden (2005). To examine these differences in greater detail, we have computed long-term averages of $\langle[u]\rangle$ and ZI for W and S years separately (Fig. 12b and Fig. 13). We begin by discussing the September and October differences. In both W and S years a poleward transition and intensification of the winds is seen from about late September, consistent with the long-term average behavior in Fig. 11. However, in S years this intensification and shift of the winds is of larger amplitude. This is particularly clear during October, where changes in ZI are found to be dominated by a reduction in zonally averaged sea level pressure at 65°S (not shown), consistent with a more poleward and intense EDJ in S years. This enhanced poleward shift of the EDJ during S years is associated with a stronger

and deeper SSPV in the stratosphere (see previous section). Thus, while the SSPV life cycle is accelerated in W years on average, it is also weaker and smaller in size, and it is the combination of these features that apparently explains why an approximate phase delay in the SSPV life cycle in S years emerges as an approximate change in amplitude (i.e., a poleward transition and intensification) in the EDJ life cycle in the troposphere during October.
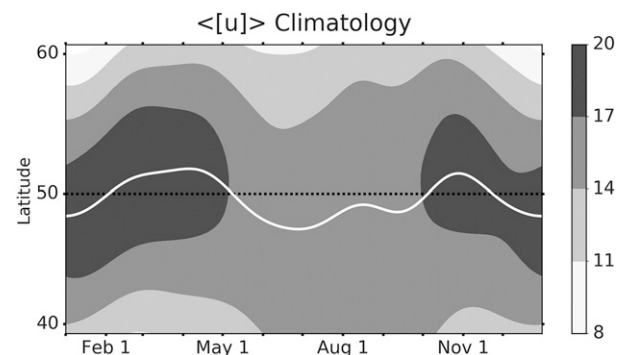

FIG. 11. Climatology of $\langle[u]\rangle$ (m s^{-1}, shading) and jet-latitude index (white line).
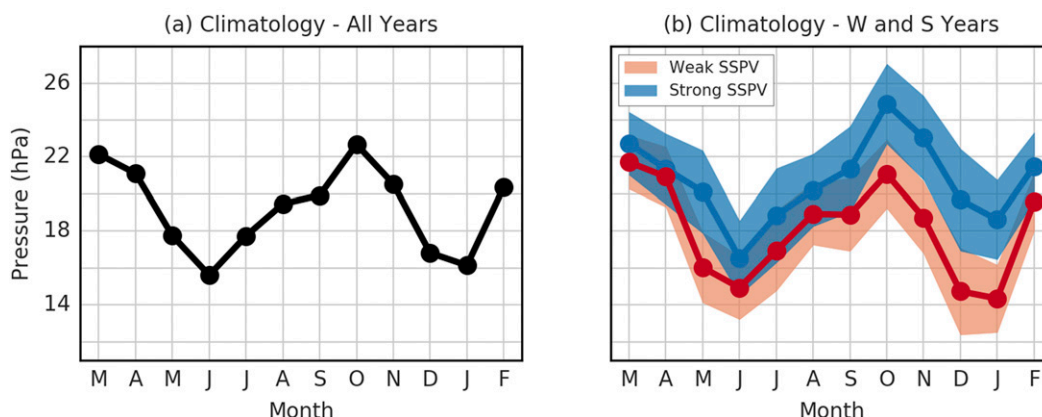
Zonal-Mean MSLP (50S - 65S)

FIG. 12. (a) Climatology of monthly mean difference in zonally averaged sea level pressure between 50° and 65°S. (b) Similar calculation for W years (red line) and S years (blue line). Shading represents a ±1.96 standard error interval for each set of years.

Between November and early February, the difference in tropospheric statistics can be largely understood in terms of the results of Byrne et al. (2017). Broadly speaking, it reflects a difference in the timing of the summer equatorward transition of the EDJ, which is closely tied to the vortex breakdown event in the stratosphere. The latter is related to the winter strength of the SSPV (see previous section). As a result, S years are on average expected to have a delayed, and somewhat reduced, equatorward transition of the EDJ compared to W years. Thus it would appear that the difference in tropospheric statistics between September and February can be approximately described as a combination of a change in amplitude (September–October–January) and a phase delay (November until January) of the EDJ life cycle, and that these

differences are closely tied to the state of the SSPV in the stratosphere.

b. Alternative circulation perspective

The results of the previous section suggest at least two components to skillful seasonal forecasting in the SH troposphere during spring and summer. The first component represents a change in the September–October EDJ statistics in association with the apparent downward merger of the SSPV and the EDJ. The second component represents a change in the November–February EDJ statistics in association with the timing and type of stratospheric vortex breakdown event. Based on our analysis in section 3, this would suggest that skillful seasonal forecasts of the troposphere might be possible based on knowledge of the state of the winter
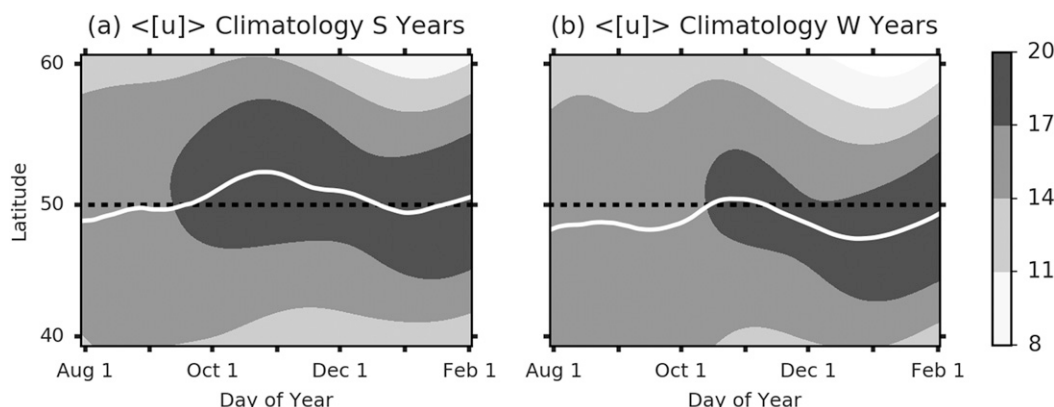

FIG. 13. (a) Climatology of ⟨[u]⟩ (m s^{-1}, shading) and jet-latitude index (white line) for S years between 1 Aug and 1 Feb. (b) Similar calculation for W years. Jet-latitude index climatologies have also been smoothed using a moving-average filter for presentation purposes.
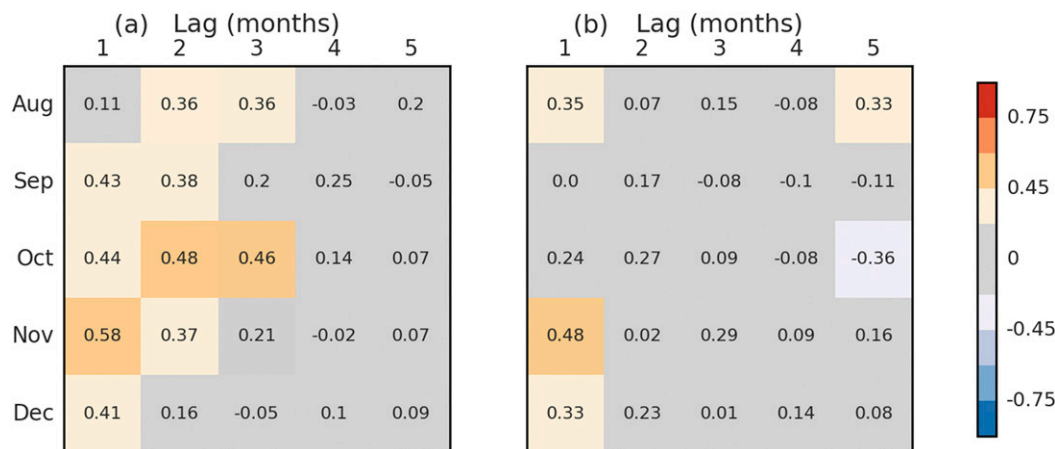
FIG. 14. (a) Correlation coefficients between polar-cap-averaged 30-hPa geopotential height at a given month of the year with ZI in the subsequent months. (b) Correlation coefficients between ZI at a given month of the year with ZI in the subsequent months. Data have been linearly detrended for each month prior to calculation in both figures. Cells that are not shaded gray represent values that are statistically significant at the 5% level based on the one-sided Student's t test. The year 2002 is not included in the correlation analysis (see text).

SSPV. To test this hypothesis, we repeat a similar analysis from section 3 and compute correlation coefficients between a measure of the SSPV at a given month of the year and a measure of the troposphere at subsequent months. We use polar-cap-averaged geopotential height at 30 hPa and the ZI time series as our respective measures. The results of this calculation for August–December are presented in Fig. 14a. Statistically significant correlations are seen to emerge for predictions of the troposphere from October until January. Furthermore, when this calculation is repeated using the troposphere as a predictor of itself (Fig. 14b) the correlations are seen to largely vanish. This is consistent with previous work by Gerber et al. (2010), who used an annular mode index to highlight that at this time of the year the stratosphere is a better predictor of the troposphere than is the troposphere itself.

As an alternative measure of the potential for skillful seasonal forecasting in the SH troposphere we provide an update of the annular mode dripping paint plots (Thompson et al. 2005; Figs. 15a,b). Although the annular modes are usually defined via an EOF analysis, the leading principal component time series is closely related to polar-cap-averaged geopotential height (Baldwin and Thompson 2009). As such, much of the behavior in Figs. 15a,b can be interpreted using the analysis from earlier sections. Inspection of these figures reveals a coherent descent of circulation anomalies in the stratosphere, with weak vortex years associated with persistent positive anomalies and with the opposite behavior for strong vortex years. This behavior is consistent with a phase delay in the shift-down of the SSPV between W and S years (see section 3). Furthermore,

both weak and strong vortex years are seen to exhibit substantial intraseasonal coherence in the troposphere, consistent with coupled variability between the stratosphere and troposphere (see previous subsection) and supporting the claim of a concomitant potential for skillful seasonal forecasting in the troposphere.

The intraseasonal coherence of anomalies in the troposphere and stratosphere suggests that annular mode anomalies have a strong synchronization with the seasonal cycle during this time of year. As a check of this statement, we have computed a plot of weak and strong vortex years as a function of calendar day of the year (Figs. 15c,d). The anomalies in these calendar year plots are seen to be of a similar magnitude and pattern as those in the previous "lag" plots. This suggests that the time-scale separation implicitly assumed in a description of circulation variability as (stationary stochastic) anomalies about a slowly varying seasonal cycle is not well satisfied during this time of year. In particular, the long intraseasonal persistence of the anomalies suggests that variations are more naturally viewed as shifts in the seasonal cycle rather than as anomalies about a seasonal cycle. Thus, combining the results from this and previous sections of the paper, we are led to propose an alternative perspective for circulation variability between September and February. We argue that during this time of year, variability of the large-scale extratropical tropospheric and stratospheric circulations is most naturally viewed as a shift in the seasonal cycle of a single, coupled entity and that the statistics of this variability can be determined by conditioning on the stratospheric circulation from the preceding winter. We note the close similarity between this perspective and those proposed
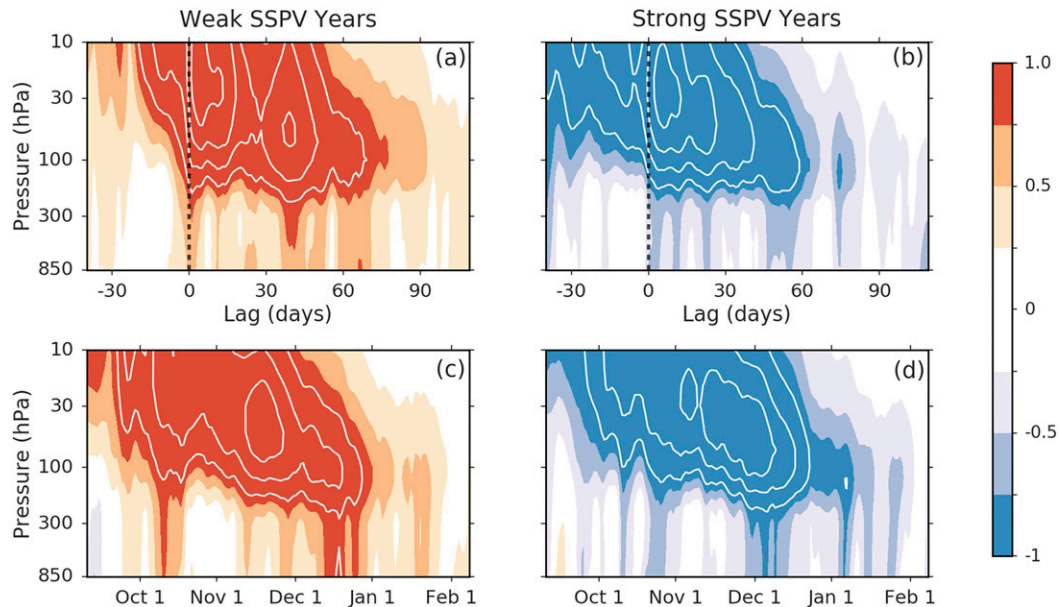
FIG. 15. Composite plots of annular mode indices for the (a) 13 weakest and (b) 13 strongest SSPV years. Weak and strong years are defined using the annular mode index at 30 hPa. Dashed vertical line represents onset date (see text). The color shading interval is 0.25 standard deviations and the contour interval is 0.5 standard deviations. Shading is drawn for values $> \pm 0.25$ standard deviations. (c),(d) As in (a),(b), but for the calendar day of the year.

by Kuroda and Kodera (1998) and Hio and Yoden (2005) using earlier versions of reanalysis products.

5. Summary and discussion

We have considered the statistical predictability of the SH stratospheric polar vortex breakdown event, using reanalysis data. We have focused on the time period from August until February, which is associated with the shift-down of the SSPV from its midwinter position. We have also considered coupled variations between the troposphere and stratosphere during this time. Our results can be broken down into three different components.

First, we have presented evidence for statistical predictability of the stratospheric polar vortex breakdown event arising from persistent variations of the SSPV in the preceding winter and spring. Evidence of statistical predictability is found from August, with maximum predictability emerging around October. This memory of (stratospheric) initial conditions over the course of several months is notable as being significantly longer than time scales that have previously been associated with atmospheric initial condition skill (Kirtman and Pirani 2007). A relationship between perturbations to the winter SSPV and the phase of the midwinter QBO has also been documented, consistent with previous results (Anstey and Shepherd 2014, and references therein). This relationship, along with a similar relationship between ENSO and the SSPV (see Byrne et al. 2017), may represent an important source of interannual variability for the SSPV.

A separate potential source of interannual variability for the SSPV has been suggested by the distribution of extreme years of our PC1 index (Fig. 4). Extreme weak years of the SSPV are found to have a tendency to directly follow extreme strong years ($p \sim 0.06$; see appendix), suggesting that memory of the SSPV can occasionally persist from one year to the next. This is reminiscent of an earlier model result of Scott and Haynes (1998). In addition, extreme years of our PC1 index, of both signs, are found to be clustered in the second half of our dataset ($p \sim 0.02$; see appendix). Ozone depletion has led to a delay in the SSPV breakdown through the satellite record, which on its own would increase the number of negative values. However, there is also a large number of positive values. It may be the case that a feedback between ozone and SSPV dynamics has increased the likelihood of extreme SSPV events during this period. A similar remark has previously been made in Black and McDaniel (2007), where the authors noted an apparent increase in interannual variability of the SSPV during later years of the satellite era.

The second component to our results builds on previous work by Kuroda and Kodera (1998) and Hio and

Yoden (2005), who documented coupled variability between the stratosphere and troposphere during austral spring and early summer. We have presented evidence for the statistical predictability of variations in the troposphere during this time, based on knowledge of the stratospheric initial state; moreover, this predictability is seen to largely vanish when the troposphere is used as a predictor of itself (see also Gerber et al. 2010). The physical explanation for this tropospheric skill can be traced to seasonal shifts in latitude of the EDJ: strong SSPV years are associated with an enhanced poleward transition in September/October and a delayed equatorward transition between November and January, with opposite behavior in weak SSPV years.

Related to this, recent research has provided evidence of model skill in forecasting the poleward transition of the EDJ, based on a model initialization in early August (Seviour et al. 2014). The present work suggests that such skill should also be realizable in forecasting the equatorward transition of the EDJ, particularly for a model initialization in early November. The use of a similar diagnostic to that proposed by Newman (1986) may represent a helpful tool for assessing model fidelity around the time of this equatorward transition. The original diagnostic of Newman (1986) considered the difference between 30-hPa zonal-mean temperature at 80° and 50°S. We find that if this diagnostic is instead defined at the 125-hPa level, the result is an almost identical time series for the stratospheric vortex breakdown date as that considered in the present study. The benefit of this alternative diagnostic is that it does not require that the SSPV breakdown event be defined in terms of a single threshold value. While the threshold definition appears to work well for the real atmosphere (Black and McDaniel 2007; Byrne et al. 2017), it may be the case that it is less suitable for a model with an unrealistic climatology.

There is evidence that the benefit of skillful forecasting of the equatorward transition of the EDJ can be quite substantial (see Byrne et al. 2017; Fig. 1). As a very recent example, we highlight the unprecedented retreat of Antarctic sea ice during 2016 (Turner et al. 2017). Sea ice decrease during this season was closely linked to high-latitude circulation anomalies; in particular, the November SAM was notable for assuming its most negative value during the satellite era. Such a large negative value appears to have been closely associated with the equatorward transition of the EDJ, which was one of the earliest during the satellite era (see Table 1). Thus, the weak SSPV of 2016 and the exceptionally early transition of the EDJ may offer a partial explanation to the puzzling behavior of sea ice during that year (Turner and Comiso 2017). Furthermore, it implicates

the stratosphere as a potentially important source of low-frequency variability in variations of Antarctic sea ice extent.

The poleward and equatorward transition of the EDJ in spring and summer is part of a broader semiannual oscillation of the EDJ (van Loon 1967). The SAO has previously been interpreted as a largely baroclinic phenomenon, emerging as a result of contrasting seasonal evolutions of surface temperature over the Southern Ocean and the Antarctic regions (see also Karoly and Vincent 1998). Our work emphasizes the additional role of the stratosphere in a complete theory for the SAO, at least between September and February. Such a role for the stratosphere has previously been considered by Bracegirdle (2011). We further note that the impact of stratospheric ozone depletion offers a natural explanation for the documented modulation of the SAO during the second half of the year since the 1970s (Hurrell and van Loon 1994). In light of recent research that has implicated stratospheric circulation changes in long-term EDJ changes in May (Ivy et al. 2017), it may also be of interest to explore the potential role of the stratosphere in EDJ behavior during the first half of the calendar year.

The third and final component to our results again builds on previous work by Kuroda and Kodera (1998) and Hio and Yoden (2005). Based on our earlier results, we have proposed an alternative perspective for large-scale SH extratropical circulation variability between September and February. We argue that during this time of year, variability is most naturally viewed not as anomalies about a climatology, but rather as a shift in the seasonal cycle of a single, coupled entity, and that the statistics of this variability can be determined by conditioning on the stratospheric circulation in the preceding winter. There are several examples where this perspective may shed new light.

First, this perspective suggests that long annular mode time scales during austral spring and summer should not be interpreted as an increased persistence of perturbations to some slowly varying seasonal cycle. Rather, it suggests that they instead reflect a phase shift of the seasonal cycle. An instructive example of the differences between these two statements can be found by considering the increased persistence seen in annular mode time scales in the troposphere during austral summer (Gerber et al. 2010). From the perspective of perturbations to some slowly varying seasonal cycle, this increased persistence has been argued to arise from eddy feedbacks in the troposphere (e.g., Kidston et al. 2015). In our proposed perspective, the increased persistence reflects year-to-year variability in the phase of the seasonal cycle (i.e., in the equatorward transition of the jet);

it is not necessarily evidence of an eddy feedback in the troposphere [see Byrne et al. (2017) for further discussion]. Note that the lag correlation between the SAM and eddy momentum flux convergence cannot be interpreted as evidence in favor of an eddy feedback (Byrne et al. 2016).

A second example of the insight offered by this perspective relates to the results of Byrne et al. (2016). In that study it was noted that SAM anomalies (along with the associated eddy momentum flux anomalies) persisted for longer during austral spring and early summer than in any other season. The present perspective offers a natural explanation for this increased persistence of circulation anomalies. Furthermore, it also suggests a hypothesis for the quasi-two-year peak of the SAM that was noted in Byrne et al. (2016): perturbations to the SSPV life cycle during winter emerge as persistent anomalies in the tropospheric circulation every year between September and February, resulting in a pronounced harmonic of the annual cycle in the SAM index. Low-frequency perturbations to the SSPV (such as the QBO or ENSO) can then excite these harmonics, with the quasi-two-year peak being the highest-frequency such harmonic. It is left to future work to establish the validity of this hypothesis.

We conclude by noting that the perspective of circulation variability originally proposed by Kuroda and Kodera (1998) and Hio and Yoden (2005) also considered the early and midwinter months of the year. These months have not been considered in the present work. Thus it may be the case that the perspective on circulation variability proposed in this paper can also be extended to other months of the year. In this respect, the month of July looks most promising [see also Kuroda and Kodera (1998) for a more detailed discussion]. In the stratosphere, July is notable as the time of year where the SSPV undergoes its annual poleward shift from subtropical to polar latitudes (e.g., Shiotani et al. 1993). In the troposphere, July is notable for large interannual variability in the location of the EDJ (e.g., Trenberth 1984). It would be of interest to determine the extent of the relationship between these two quantities; however, it should be noted that as a result of the low-latitude position of the SSPV during much of July, Annular Mode (i.e., polar cap) diagnostics may not be the optimum measure of circulation variability for this time of year. We also draw attention to the theoretical work of Scott and Haynes (2000, 2002), which suggests that the late winter configuration of the SSPV (i.e., the emergence of W or S years) can often be traced back to the early winter wave forcing [see also Shiotani et al. (1993) for some observational support of this statement]. The year of 2002 would appear to be a particular example of such a scenario (Harnik et al. 2005).

APPENDIX

Statistical Significance Tests

To quantify whether extreme values of our PC1 index are clustered in the second half of our dataset we proceed as follows. First we generate a synthetic time series of 18 ''0s'' and 20 ''1s''. These zeros and ones are randomly distributed within the time series and are intended to mimic extreme events in our original PC1 index (which contains 20 extreme events). Next, we calculate the difference between the sum of the first 19 elements and the remaining 19 elements of this synthetic time series to arrive at a value d. Finally, we repeat this calculation 10^6 times to form a distribution for d. The difference for our PC1 time series is $d = 8$. According to our synthetic distribution, the probability of $|d| \geq 8$ is $p \sim 0.02$.

To quantify whether extreme positive values of our PC1 index have a tendency to follow extreme negative years we proceed as follows. First we generate a synthetic time series of ten ''-1s'' and ten ''$+1$s''. These -1s and $+1$s are randomly distributed within a time series of length 38, padded with zeros, and are intended to mimic extreme negative and extreme positive events in our original PC1 index. Next, we derive a new time series by forming the difference between adjacent entries in our original synthetic time series. For example, if the first and second entries of our synthetic time series are -1 and $+1$, respectively, the first entry of our derived time series will be $+2$. Once we have constructed our derived time series, we count the number of occurrences of $+2$ in this time series; $+2$ is a unique

identifier of an extreme positive event directly following an extreme negative event. Finally, we repeat this calculation 10^6 times to form a distribution. The number of $+2s$ in our PC1 time series is 5. According to our synthetic distribution, this has an approximate p value of $p \sim 0.06$.

To determine whether there is a statistical relationship between the phase of the QBO and our PC1 index, we first note that 15 easterly QBO years have been associated with positive PC1 years and 6 easterly QBO years have been associated with negative PC1 years (by symmetry this calculation will be the same for westerly QBO years). We then test the statistical significance of this configuration using a hypergeometric sampling distribution, with the result being an approximate p value of 0.06.

REFERENCES

Anstey, J. A., and T. G. Shepherd, 2014: High-latitude influence of the quasi-biennial oscillation. *Quart. J. Roy. Meteor. Soc.*, **140**, 1–21, https://doi.org/10.1002/qj.2132.

Baldwin, M. P., and T. J. Dunkerton, 1998: Quasi-biennial modulation of the Southern Hemisphere stratospheric polar vortex. *Geophys. Res. Lett.*, **25**, 3343–3346, https://doi.org/10.1029/98GL02445.

——, and D. W. J. Thompson, 2009: A critical comparison of stratosphere–troposphere coupling indices. *Quart. J. Roy. Meteor. Soc.*, **135**, 1661–1672, https://doi.org/10.1002/qj.479.

Black, R. X., and B. A. McDaniel, 2007: Interannual variability in the Southern Hemisphere circulation organized by stratospheric final warming events. *J. Atmos. Sci.*, **64**, 2968–2974, https://doi.org/10.1175/JAS3979.1.

Bracegirdle, T. J., 2011: The seasonal cycle of stratosphere-troposphere coupling at southern high latitudes associated with the semi-annual oscillation in sea-level pressure. *Climate Dyn.*, **37**, 2323–2333, https://doi.org/10.1007/s00382-011-1014-4.

Butler, A. H., and Coauthors, 2016: The climate-system historical forecast project: Do stratosphere-resolving models make better seasonal climate predictions in boreal winter? *Quart. J. Roy. Meteor. Soc.*, **142**, 1413–1427, https://doi.org/10.1002/qj.2743.

Byrne, N. J., 2017: Deterministic models of Southern Hemisphere circulation variability. Ph.D. thesis, University of Reading, 105 pp.

——, T. G. Shepherd, T. Woollings, and R. A. Plumb, 2016: Annular modes and apparent eddy feedbacks in the Southern Hemisphere. *Geophys. Res. Lett.*, **43**, 3897–3902, https://doi.org/10.1002/2016GL068851.

——, ——, ——, and ——, 2017: Nonstationarity in Southern Hemisphere climate variability associated with the seasonal breakdown of the stratospheric polar vortex. *J. Climate*, **30**, 7125–7139, https://doi.org/10.1175/JCLI-D-17-0097.1.

Dee, D. P., and Coauthors, 2011: The ERA-Interim reanalysis: Configuration and performance of the data assimilation system. *Quart. J. Roy. Meteor. Soc.*, **137**, 553–597, https://doi.org/10.1002/qj.828.

Fioletov, V. E., and T. G. Shepherd, 2003: Seasonal persistence of midlatitude total ozone anomalies. *Geophys. Res. Lett.*, **30**, 1417, https://doi.org/10.1029/2002GL016739.

Gerber, E. P., and Coauthors, 2010: Stratosphere-troposphere coupling and annular mode variability in chemistry-climate models. *J. Geophys. Res.*, **115**, D00M06, https://doi.org/10.1029/2009JD013770.

Harnik, N., R. K. Scott, and J. Perlwitz, 2005: Wave reflection and focusing prior to the major stratospheric warming of September 2002. *J. Atmos. Sci.*, **62**, 640–650, https://doi.org/10.1175/JAS-3327.1.

Hartmann, D. L., C. R. Mechoso, and K. Yamazaki, 1984: Observations of wave-mean flow interaction in the Southern Hemisphere. *J. Atmos. Sci.*, **41**, 351–362, https://doi.org/10.1175/1520-0469(1984)041<0351:OOWMFI>2.0.CO;2.

Hio, Y., and S. Yoden, 2004: Quasi-periodic variations of the polar vortex in the Southern Hemisphere stratosphere due to wave–wave interaction. *J. Atmos. Sci.*, **61**, 2510–2527, https://doi.org/10.1175/JAS3257.1.

——, and ——, 2005: Interannual variations of the seasonal march in the Southern Hemisphere stratosphere for 1979–2002 and characterization of the unprecedented year 2002. *J. Atmos. Sci.*, **62**, 567–580, https://doi.org/10.1175/JAS-3333.1.

Hirano, S., M. Kohma, and K. Sato, 2016: A three-dimensional analysis on the role of atmospheric waves in the climatology and interannual variability of stratospheric final warming in the Southern Hemisphere. *J. Geophys. Res. Atmos.*, **121**, 8429–8443, https://doi.org/10.1002/2015JD024481.

Hirota, I., K. Kuroi, and M. Shiotani, 1990: Midwinter warmings in the Southern Hemisphere stratosphere in 1988. *Quart. J. Roy. Meteor. Soc.*, **116**, 929–941, https://doi.org/10.1002/qj.49711649407.

Hitchcock, P., T. G. Shepherd, and G. L. Manney, 2013: Statistical characterization of Arctic polar-night jet oscillation events. *J. Climate*, **26**, 2096–2116, https://doi.org/10.1175/JCLI-D-12-00202.1.

Hurrell, J. W., and H. van Loon, 1994: A modulation of the atmospheric annual cycle in the Southern Hemisphere. *Tellus*, **46A**, 325–338, https://doi.org/10.3402/tellusa.v46i3.15482.

Ivy, D. J., C. Hilgenbrink, D. Kinnison, R. A. Plumb, A. Sheshadri, S. Solomon, and D. W. J. Thompson, 2017: Observed changes in the Southern Hemispheric circulation in May. *J. Climate*, **30**, 527–536, https://doi.org/10.1175/JCLI-D-16-0394.1.

Karoly, D. J., and D. G. Vincent, 1998: *Meteorology of the Southern Hemisphere*. Meteor. Monogr., No. 49, Amer. Meteor. Soc., 410 pp.

Kidson, J. W., 1988: Indices of the Southern Hemisphere zonal wind. *J. Climate*, **1**, 183–194, https://doi.org/10.1175/1520-0442(1988)001<0183:IOTSHZ>2.0.CO;2.

Kidston, J. W., A. A. Scaife, S. C. Hardiman, D. M. Mitchell, N. Butchart, M. P. Baldwin, and L. J. Gray, 2015: Stratospheric influence on tropospheric jet streams, storm tracks and surface weather. *Nat. Geosci.*, **8**, 433–440, https://doi.org/10.1038/ngeo2424.

Kirtman, B., and A. Pirani, 2007: WCRP position paper on seasonal prediction. WCRP Informal Rep. 3/2008 ICPO Publ. 127, 25 pp.

Kuroda, Y., and K. Kodera, 1998: Interannual variability in the troposphere and stratosphere of the Southern Hemisphere winter. *J. Geophys. Res.*, **103**, 13 787–13 799, https://doi.org/10.1029/98JD01042.

National Research Council, 2010: *Assessment of Intraseasonal to Interannual Climate Prediction and Predictability*. National Academies Press, 181 pp.

Newman, P. A., 1986: The final warming and polar vortex disappearance during the Southern Hemisphere spring.

Geophys. Res. Lett., **13**, 1228–1231, https://doi.org/10.1029/GL013i012p01228.

North, G. R., T. L. Bell, and R. F. Cahalan, 1982: Sampling errors in the estimation of empirical orthogonal functions. *Mon. Wea. Rev.*, **110**, 699–706, https://doi.org/10.1175/1520-0493(1982)110<0699:SEITEO>2.0.CO;2.

Palmer, T. N., and D. L. T. Anderson, 1994: The prospects for seasonal forecasting—a review paper. *Quart. J. Roy. Meteor. Soc.*, **120**, 755–793, https://doi.org/10.1002/qj.49712051802.

Roscoe, H. K., J. D. Shanklin, and S. R. Colwell, 2005: Has the Antarctic vortex split before 2002? *J. Atmos. Sci.*, **62**, 581–588, https://doi.org/10.1175/JAS-3331.1.

Scott, R. K., and P. H. Haynes, 1998: Internal interannual variability of the extratropical stratospheric circulation: The low-latitude flywheel. *Quart. J. Roy. Meteor. Soc.*, **124**, 2149–2173, https://doi.org/10.1002/qj.49712455016.

——, and ——, 2000: Internal vacillations in stratosphere-only models. *J. Atmos. Sci.*, **57**, 3233–3250, https://doi.org/10.1175/1520-0469(2000)057<3233:IVISOM>2.0.CO;2.

——, and ——, 2002: The seasonal cycle of planetary waves in the winter stratosphere. *J. Atmos. Sci.*, **59**, 803–822, https://doi.org/10.1175/1520-0469(2002)059<0803:TSCOPW>2.0.CO;2.

Seviour, W. J. M., S. C. Hardiman, L. J. Gray, N. Butchart, C. Maclachlan, and A. A. Scaife, 2014: Skillful seasonal prediction of the southern annular mode and Antarctic ozone. *J. Climate*, **27**, 7462–7474, https://doi.org/10.1175/JCLI-D-14-00264.1.

Shiotani, M., N. Shimoda, and I. Hirota, 1993: Interannual variability of the stratospheric circulation in the Southern Hemisphere. *Quart. J. Roy. Meteor. Soc.*, **119**, 531–546, https://doi.org/10.1002/qj.49711951110.

Sigmond, M., J. F. Scinocca, V. V. Kharin, and T. G. Shepherd, 2013: Enhanced seasonal forecast skill following stratospheric sudden warmings. *Nat. Geosci.*, **6**, 98–102, https://doi.org/10.1038/ngeo1698.

Son, S. W., A. Purich, H. H. Hendon, B. M. Kim, and L. M. Polvani, 2013: Improved seasonal forecast using ozone hole variability? *Geophys. Res. Lett.*, **40**, 6231–6235, https://doi.org/10.1002/2013GL057731.

Stockdale, T. N., F. Molteni, and L. Ferranti, 2015: Atmospheric initial conditions and the predictability of the Arctic Oscillation. *Geophys. Res. Lett.*, **42**, 1173–1179, https://doi.org/10.1002/2014GL062681.

Sun, L., G. Chen, and W. A. Robinson, 2014: The role of stratospheric polar vortex breakdown in Southern Hemisphere climate trends. *J. Atmos. Sci.*, **71**, 2335–2353, https://doi.org/10.1175/JAS-D-13-0290.1.

Thompson, D. W. J., and J. M. Wallace, 2000: Annular modes in the extratropical circulation. Part I: Month-to-month variability. *J. Climate*, **13**, 1000–1016, https://doi.org/10.1175/1520-0442(2000)013<1000:AMITEC>2.0.CO;2.

——, M. Baldwin, and S. Solomon, 2005: Stratosphere–troposphere coupling in the Southern Hemisphere. *J. Atmos. Sci.*, **62**, 708–715, https://doi.org/10.1175/JAS-3321.1.

——, S. Solomon, P. J. Kushner, M. H. England, K. Grise, and D. Karoly, 2011: Signatures of the Antarctic ozone hole in Southern Hemisphere surface climate change. *Nat. Geosci.*, **4**, 741–749, https://doi.org/10.1038/ngeo1296.

Trenberth, K. E., 1984: Interannual variability of the Southern Hemisphere circulation: Representativeness of the year of the global weather experiment. *Mon. Wea. Rev.*, **112**, 108–123, https://doi.org/10.1175/1520-0493(1984)112<0108:IVOTSH>2.0.CO;2.

Tripathi, O. P., and Coauthors, 2015: The predictability of the extratropical stratosphere on monthly time-scales and its impact on the skill of tropospheric forecasts. *Quart. J. Roy. Meteor. Soc.*, **141**, 987–1003, https://doi.org/10.1002/qj.2432.

Turner, J., and J. Comiso, 2017: Solve Antarctica's sea-ice puzzle. *Nature*, **547**, 275–277, https://doi.org/10.1038/547275a.

——, T. Phillips, G. J. Marshall, J. S. Hosking, J. O. Pope, T. J. Bracegirdle, and P. Deb, 2017: Unprecedented springtime retreat of Antarctic sea ice in 2016. *Geophys. Res. Lett.*, **44**, 6868–6875, https://doi.org/10.1002/2017GL073656.

van Loon, H., 1967: The half-yearly oscillations in middle and high southern latitudes and the coreless winter. *J. Atmos. Sci.*, **24**, 472–486, https://doi.org/10.1175/1520-0469(1967)024<0472:THYOIM>2.0.CO;2.